Journal of Enviromental Economics & Chemical Processes (JEECP)

Journal of Enviromental Economics & Chemical Processes (JEECP)

journal homepage: *WWW.JEECPJournal.com*

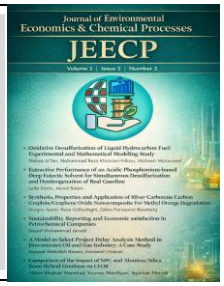

Synthesis, Properties and Appplication of Silver Carbonate Carbon Graphite/Graphene Oxide Nanocomposite For Methyl Orange Degradation

Narges Ajami* Reza Golbedaghi, Zahra Farzani Basmenj

Department of Chemistry, Payame Noor University, 19395-4697, Tehran, Iran.

P A P E R I N F O

Paper history:
Received 12/20/2024
Accepted in revised form 03/10/2025

Keywords:
Nanocomposites
Graphite Carbon Nitride
Graphene Oxide
FTIR Spectrum

A B S T R A C T

This paper examined the absorption of methyl orange dye by three graphite nitrides, graphene oxide, and silver carbonate nanocomposites. The absorption of methyl orange dye solution at 465 nm wavelength was checked by UV-VIS to determine the initial and final dye. The results showed that in different cases with increasing contact time, the amount of methyl orange absorbed per unit weight of the absorbent increased, and the absorption process was completed in different stages at different times. The maximum absorption efficiency was obtained at 15 ppm (equal to 92.5%). In this study, the effects of initial dye concentration, adsorbent dosage, pH, and contact time on the adsorption process were investigated. The optimal conditions for maximum adsorption capacity were determined to be at pH_3, an adsorbent dosage of 0.02 g/L, an initial methyl orange concentration of 15 ppm, and an equilibrium contact time of 25 minutes. Under these conditions, the experimental data were best fitted by the pseudo-second-order kinetic model. For equilibrium studies, the Langmuir and Freundlich isotherm models were applied. The adsorption data showed a better fit with the Langmuir model, indicating monolayer adsorption of methyl orange on the adsorbent surface. The ternary nanocomposite GO/AC/CN was synthesized through a simple method of chemical precipitation in the environment. The mentioned nanocomposites underwent physical tests by X-ray diffraction (XRD), energy dispersive x-ray spectroscopy (EDX), Fourier transform infrared (FTIR), XRD device, and scanning electron microscope (SEM) to determine the structural properties, surface compositions, properties and morphology following synthesis.

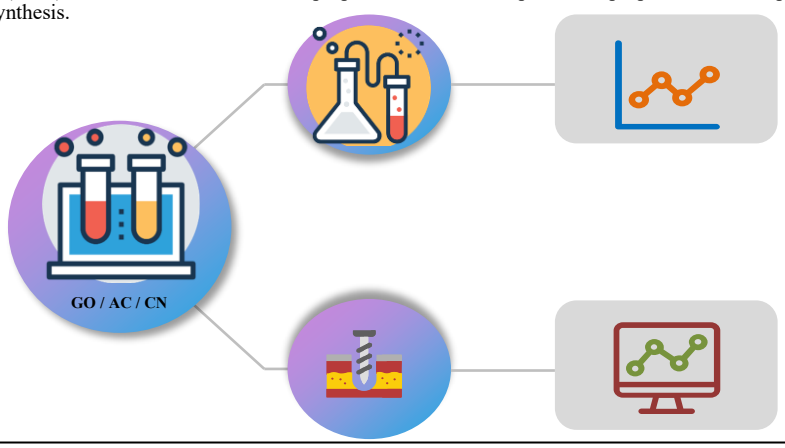

1. Introduction

Environmental pollutions are a serious concern for all countries around the word these days. The body and organism of the scientific community are directly related to humans [1]. Dangerous organic compounds such as chemicals, dyes, pesticides, etc. include the main pollutants released in liquids same as water, and these pollutions disturb the environment by increasing the beauty of liquids [2-3]. Water pollution by organic contaminants, such as synthetic dyes, is a significant environmental issue. These toxic materials must be removed or reduced to acceptable levels before being discharged into natural water bodies or reused [4]. Among various wastewater treatment ways, hotocatalysis have garnered considerable attention due to their potential to mineralize organic pollutants under solar irradiation [5]. Nanoparticles (NPs) have been recognized for their diverse applications due to their distinct physicochemical properties involving surface are, lesser sizes, high reactivity, great stability and versatile chemistry with different fictionalizations possibilities. Nanomaterial compounds have been used for wastewater treatment as one of the sustainable solutions of water crisis and NPs are being used to extend innovative tools and to improve existing technologies for the detection/prevention and remediation of water pollutions [6]. Synthetic dyes such as Methylene Blue (MB), Methyl Orange (MO), Methyl Yellow (MY), and Methyl Red (MR) are extensively have used in industries like textiles, leather tanning, paper, printing, food processing, plastics, and cosmetics [7-11]. Textile effluents released from these industries can have devastating effects on ecosystems [12,13]. Based on their ionic nature, dyes are classified into anionic, cationic, and non-ionic types. MB and MO are anionic dyes, which

* golbedaghi82@gmail.com

URL: http://jeecpjournal.ir/index.php/jeecp/article/view/15

Please cite this article as: Ajami, N., Golbedaghi, R., & Farzani Basmenj, R., (2025). *Journal of Enviromental Economics & Chemical Processes (JEECP)*, *2*(2), 49-55.

rely on negative ions and possess complex molecular structures. MB belongs to the triphenylmethane class, while MO is an azo dye. Various water treatment technologies are currently employed to remove such pollutants. Recent studies indicate that adsorption is preferred over other treatment methods due to its simplicity, low cost, flexibility, and efficiency. Not only can it effectively eliminate hazardous pollutants, but it also facilitates the recovery and recycling of industrial processes in an environmentally sustainable manner [14-16]. Different methods have been checked, involving absorption, reverse osmosis, sedimentation, advanced oxidation methods, filtration, disinfection, and other methods. Dyes are stable against some ways, especially biological methods, thus advanced oxidation ways same as photodegradation, biological degradation, and oxidizing agents include the most efficient methods for organic dyes removal [17-19]. Dyes are organic compounds that generally consist of two main functional units: chromophores, which are responsible for color, and auxochromes, which enhance solubility and assist in dye attachment to fiber surfaces. Due to their aromatic structures, dyes absorb light in the visible range (350–700 nm). Consequently, dye-containing wastewater must be treated before environmental discharge. Consid ering the associated constraints with different technologies, the adsorption process seems to be the ideal choice for most researchers nowadays [20]. It is the most common and frequently utilized for bulk wastewater treatment which provides low maintenance costs, high efficiency, low energy requirement, and ease of operation [21]. Recently, different adsorbents such as silica gel [22], alumina [23], zeolites [24], bentonite clays [25], natural polymeric bio-sorbents [26-27], activated carbon (AC) [28,29], acid modified AC [30], carbon nano fibers [31], biochar [32-35], etc. have been applied for the removal of different types of toxic dyes. Previously, researchers have identified adsorption as an effective and feasible technique to remove the dye from textile wastewater due to its superior performance, energy efficiency, cost - effectiveness, low complexities, regenerability, and reusability. In recent years, graphene oxide (GO) and GO - based composite materials have been studied as highly efficient adsorbents for removing refractory organic contaminants and other organic pollutants. Large surface area, 2 D stacked layers, and the abundance of active functional groups make GO an excellent candidate for the treatment of dye - containing wastewater. Moreover, GO is an ideal material for creating composite and functionalized materials due to the availability of different functional groups, e.g., epoxides (C - O - C), phenolic hydroxyl (-OH), carboxylic (- COOH), and other carbonyl groups (C = O) and its 2 D layered structure. Previously, several researchers have used GO for the removal of heavy metals, organic and inorganic composite contaminants, methyl orange, naphthalene, 1 - naphthol, arsenic, fluoride, and other pollutants from massive volumes of aqueous solutions (Table S1). Fraga et al [36].

Conventional biological and chemical methods are not efficient for the degradation of the dye because their molecular structure does not contain aromatic amide groups with alkyl, halogen, nitro, hydroxyl, sulfonic acid, substituents, and mineral salts. Adsorption using activated carbon is very necessary and efficient to remove dyes, but it requires a high cost for reconstruction [37,38]. More than ten thousand azo dyes are used in the textile industry having the molecular structure of the N=N- dye group which makes up the largest part of commercial paints [39]. Zollinger (2007) states that a major part of synthetic organic dyes is azo dyes, constituting half of the dyes used in today's textiles. Methyl Orange (MO), an azo dye, is widely used in the textile industry. Advanced oxidation processes (AOPs) have proven effective in degrading and removing dye molecules from industrial wastewater, including effluents from textiles, leather, paper, pharmaceuticals, and cosmetics. High concentrations of such dyes in wastewater represent a major environmental and industrial concern [40]. AC is a narrow-bandgap semiconductor photocatalyst that exhibits excellent optical and photocatalytic performance under light irradiation conditions [41]. Silver carbonate (Ag_2CO_3) is widely used for coupling with other semiconductors to enhance photocatalytic performance [42]. Among the noble metals, Ag is more cost-effective than Au, Pd, and Pt and thus selected for the investigation[43]. Activated carbon (AC), due to its high porosity and surface area, has been widely used for dye removal and significantly improves the adsorption process [44-46]. Graphitic carbon nitride CN with strong absorption capacity reduces the photocatalytic activity of high organic pollutants [47]. Graphene oxide is an excellent absorbent due to its large surface area and significant hydrophilic groups [48].The triple nanocomposite of graphite nitride carbon, graphene oxide and silver carbonate AC / CN / GO has a high adsorption range and good stability. Graphene, with its two-dimensional hexagonal honeycomb structure and sp^2 hybridization, possesses superior optical, mechanical, and electrical properties [49]. Graphene oxide (GO), on the other hand, offers enhanced electrical conductivity, higher surface area, and good mechanical stability [50]. GO nanoparticles contain active surface groups, such as hydroxyl and carboxyl functionalities, which make them suitable for composite photocatalysts (e.g., GO/AC/CN). These results suggest a promising potential for the use of such photocatalysts in water purification. Therefore, developing adsorbents with high adsorption capacity, low regeneration cost, and easy separation remains a key objective for environmental researchers.

2. Method

All the chemicals used in the experiments were procured from merk company, Germany. The g-C_3N_4 nanoparticles were synthesized using the same method as mentioned in a previously manuscripts [51]. 5 gr of white melamine powder inside a porcelain mug was heated for 4 hours in a muffle furnace at a temperature of 560 ◦C. The next day, a yellow and hard material called Graphite Carbon Nitride (g-C_3N_4) has been formed after reaching the room temperature. Then, we grind the material in a mortar until it turns into a powder. GO was prepared from purified natural graphite powder according to the modified Hummers' method [52]. We place a 1000 ml flask under the hood in an ice water bath. Then we add 90 ml of sulfuric acid, and then we added 6 gr of sodium nitrate and 6 gr of graphite. The resulting mixture was stirred in an ice water bath for 4 hours, and then we turned on the hood and added 18 gr of potassium permanganate (in two parts, 9 gr each time, half an hour apart). After adding permanganate, half an hour later, we removed the ice bath so that the reaction continues at room temperature. We consider the rotation of the magnet to be slow. After two days, we slowly added 300 ml of distilled water to the reaction mixture from the flask wall. (Hood should be on). The reaction temperature was adjusted to 90 to 98 degrees after two hours. Then we added another 450 ml of water and let it spin for 2 hours. We added 30 ml of hydrogen peroxide and its color turns yellow. After two hours, we added 15 ml of concentrated hydrochloric acid and the reaction ends. After 24 hours, we drain the water on the sediment and centrifuge the resulting sediment and place it in an ultrasonic bath at room temperature for 30 minutes. (The ultrasonic was done because the graphit layers on graphene oxide to be separated and the product will be single-layer and nano). After that, we centrifuged the ultrasonic sediment, and then we added acetone to the sediment at the bottom of the tube to the half of the tube, and the acetone overflows and the final sediment were obtained. By this way, we taked out the sediment from the tubes and pour it into glass petri dishes and place it inside the oven at a temperature of 50 to 60 degrees until it dries. The resulting sediment can be used as graphene oxide sheet or graphene oxide powder. 0.04 gr of graphene oxide powder synthesized by Hammers method and 1 gr of yellow graphite carbon nitride powder were added respectively in 100 ml of deionized water with a stirrer. It was placed on the stirrer (magnetic stirrer) for 1 hour, then 1.2318 gr of AgNO3 along with 36.26 ml of 0.1 mol Na_2CO_3 (solution) was added to it and placed in the ultrasonic device for 30 minutes. The solution was placed on the stirrer for 1 hour so that $Ag+$ and CO_3^{-2} ions are well absorbed or dispersed on the surface. Later on, stirring continued for an hour in the dark. After this step, the solution was placed in a centrifuge, washed with deionized water, collected and dried in an oven at a 60°C [53]. To prepare 200 ppm of the concentration of methyl orange dye solution, 0.05 grams of methyl orange powder was added in a 250 cc flask. Two-beam UV-VIS spectrophotometer device and its absorption characteristics at visible-ultraviolet region was used to measure the MO concentration. The absorption spectrum of methyl orange has a strong absorption at 465 nm wavelength, which is the same wavelength λ max was chosen to measure the concentration. The mechanism of methyl orange dye degradation same. The mechanism of methyl orange degradation proceeds through two pathways: degradation of the conjugated structure and removal of dimethyl. If the hydroxyl radical attacks nitrogen, the demethylation pathway proceeds, and if it attacks the aromatic ring, the conjugated structure degradation pathway proceeds. It is clear from the figure that the dye produces intermediates during the degradation process and is ultimately converted into water and carbon dioxide as the final products [52].

3. Results and Discussion

After the synthesis of the nanocomposite, its properties were investigated by various methods such as X-ray diffraction (XRD), transmission electron microscope (TEM), scanning electron microscope (SEM), spectrometer (EDX) and infrared Fourier transform (IR-FT). Then, its photocatalytic property was evaluated in the degradation of methyl orange dissolved in water under visible light radiation. The effect of the concentration of methyl orange (MO) dye, the mass of the photocatalyst, the solution pH, and the frequency of use of the nanocomposite without reducing the photocatalytic activity were investigated.

To analyze the crystalline structure of the synthesized nanoparticles, X-ray diffraction (XRD) spectroscopy was employed. The instrument used in this study was the SHIMADZU XRD-6000 equipped with CuKα radiation (λ = 1.54 Å). The crystallite size from the observed diffraction peaks was calculated using the Scherrer equation [54] as follows: $D = \frac{K\lambda}{\beta cos\theta}$

The average crystallite size obtained from this equation for the synthesized nanocomposite was 50 nm. Similarly, the calculated sizes for synthesized graphene oxide and graphitic carbon nitride were 37 nm and 40 nm, respectively [Fig. 1].

The index peaks (Figure1) of carbon, nitrogen, oxygen and silver elements with atomic percentages of 39.47%, 44.77%, 35.25% and 23.01% show respectively for the synthesis of graphite carbon nitride, graphene oxide and ternary nanocomposite AC/GO/CN.

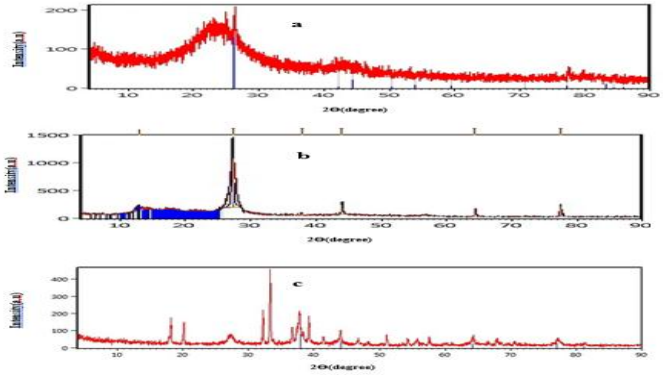

Figure 1. XRD pattern of graphene oxide GO(a), XRD pattern of C3N4 graphite nitride carbon(b), and XRD pattern of Ag2CO3 / GO / C3N4 triple nanocomposite(C)

The observed peaks at an angle of 10 degrees correspond to (001) crystal planes (Fig.1a). Also, the peak observed at 26 degrees confirms the presence of graphite in the sample. It should be noted that the observed peaks at angles of 21 and 43 degrees correspond to crystal planes (101), which is caused by the reflection of graphene oxide from graphite. This phenomenon is due to the presence of oxygen functional groups on the graphene oxide/ graphene layers surface.

The pattern shown in Fig.1b is related to graphene carbon nitride particles. According to the reference card JCPDS card 87-1526, the peaks created at angles of 12.72 and 27 degrees correspond to (110) and (002) crystal planes. The X-ray diffraction shown in Fig.1c confirms the formation of the composite. According to the figure, it is clear that the peaks related to graphene oxide and graphene nitride have appeared in their place. According to JCPDS reference card No. 1236-31, the peaks observed at the angles of 18, 20, 34, 35, 40, 53, 61 and 68 correspond to the crystal planes (101), (110), (211), (300), (220), (222), (410), (330) and (304), respectively, confirming the presence of silver carbonate particles in the composite structure. It should be noted that according to JCPDS reference card No. 01-087-0719, the peaks appearing at angles of 38, 44, 64 and 75 correspond to the presence of metallic silver particles that correspond to the crystal planes (111), (200), (220) and (311). The basis of FTIR spectroscopy is the ability of different molecular vibrations to absorb energy in the infrared spectral range 14000-400 cm^{-1} for vibrational transitions. In the infrared spectrum, the latitudinal axis shows the radiation intensity in percentage and the length axis shows the wave number corresponding to the wavelength of the infrared light emitted in cm^{-1}. The lower the amount of transmitted radiation in a certain wave number, the higher the absorption of radiation by the related bond. The amount of absorption is higher in a polar bond, and as a result the peak is longer (less crossing). The wave number of each peak shows the presence of a specific functional group in the sample. The location of the absorption peak of different functional groups in the Spectroscopy books and various references are available in the form of correlation tables. In this paper, the samples were mechanically mixed with KBr powder and pressed into the disc to obtain the FT-IR spectra.

As can be seen in Figure 2a, several peaks in the range of CM^{-1} 1600-11000 are assigned to the normal oscillation of CN anomalous rings. The absorption peaks in 1638 CM^{-1} and 1238 CM^{-1} are attributed to C and C-N stretch states, respectively. There are also broad bands of stretching and deformation modes of the group as well as an overlapping band of the O-H CM^{-1} group in the range of -1 3414 CM.

The FTIR spectrum (Fig. 2b) was divided into two broad absorption bands for CN[2b]. Peak absorption included 3000- 3400 CM^{-1}, 1200-1700 CM^{-1} and 800 CM^{-1} wide band in 300-3400 CM^{-1} was due to stretching modes. NH2 or NH end groups in the aromatic ring position have broad peaks at 1200-1700 CM^{-1} and 800 CM^{-1} due to the skeletal vibrations of C-N aromatic heterocycles and the stretching vibration of triazine units. The pure AC spectrum, which is clearly observed, has a broad peak in the range of 3500 CM^{-1}, which is attributed to the O-H vibration. In addition, the absorption peak of $C O_3^{-2}$ is observed in 1705،880،1370،1440 CM^{-1}. Compared with the AC spectrum, the AC/GO spectrum has a significant change in the range of 1300-1500 CM^{-1}. The change of the chemical environment of AC is due to the addition of GO. FTIR spectra of CN/AC and CN/AC/GO shows pure overlap. AC and CN spectra indicate the coexistence of two semiconductors and the formation of a ternary catalyst. The absorption spectrum (Fig. 2c) in 1728 CM^{-1} is attributed to the asymmetric stretching of carbonyl C=O (carboxylic acid), while the peaks corresponding to 1630 CM-1and 1072 CM^{-1} indicate epoxy and alkoxy C-O groups, respectively. The peaks corresponding to 3430 CM^{-1} are O-H bond and 1044 CM^{-1} correspond to C-O.

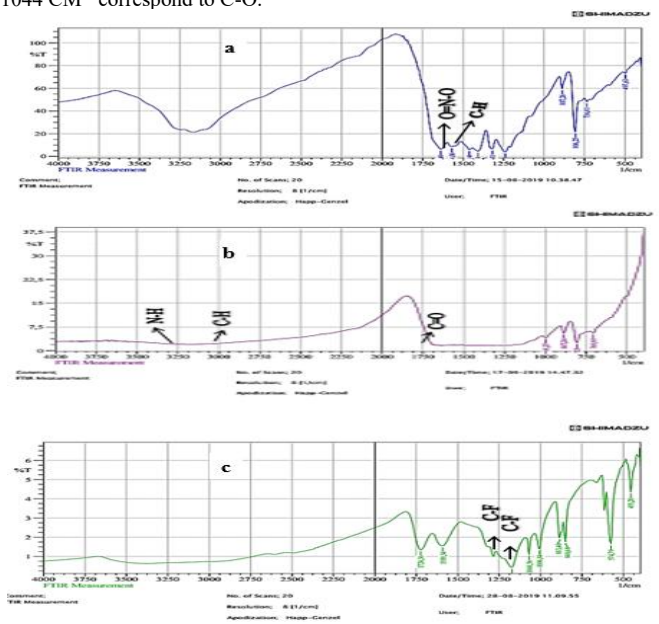

Figure 2. Graphite carbon nitride FTIR diagram(a), AC / GO/CN triple nanocomposite(b), Graphite oxide FTIR diagram(c)

The results of surface and morphology measurements of graphitic carbon nitride, graphene oxide, and the AC/GO/CN ternary adsorbent are shown in Fig. 3. The top three patterns (3a) are for graphitic carbon nitride, the middle three patterns (3b) are for graphene oxide, and the bottom three patterns (3c) are for the AC/GO/CN adsorbent. As shown in the figure, the ternary nanocomposite has larger particles and a smoother surface, and after the synthesis of the adsorbent, these flat particles have been transformed into particles with a larger cross-sectional area. The adsorbent surface exhibits more pores and a more suitable grain size; this feature increases the efficiency of the adsorbent for absorbing and trapping methyl orange pollutant particles.

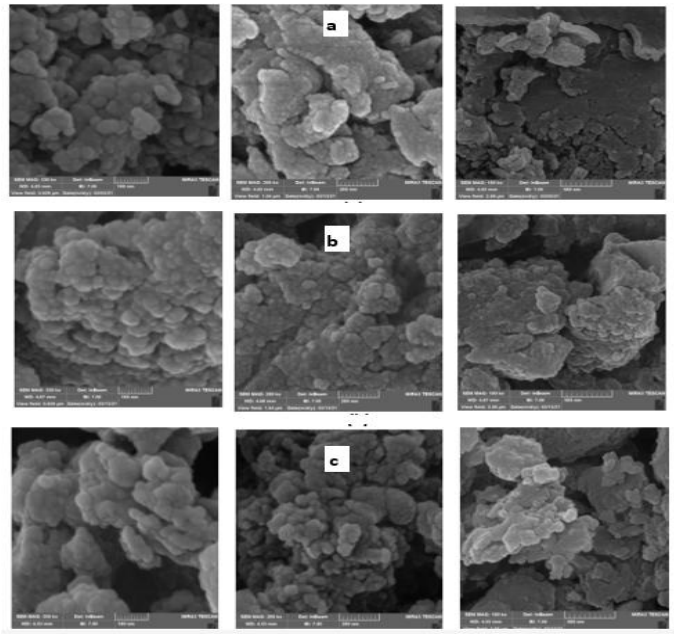

Figure 3. SEM image (a) Graphite carbon nitride, (b) Graphene oxide, (c) Triple nanocomposite with magnification 100,200,500

EDAX analysis shows peaks indicative of carbon, nitrogen, oxygen, and silver elements with atomic percentages of 39.47%, 44.77%, 35.25%, and 23.01%, respectively, for the synthesis of graphitic carbon nitride, graphene oxide, and AC/GO/CN ternary nanocomposite [Fig. 4].

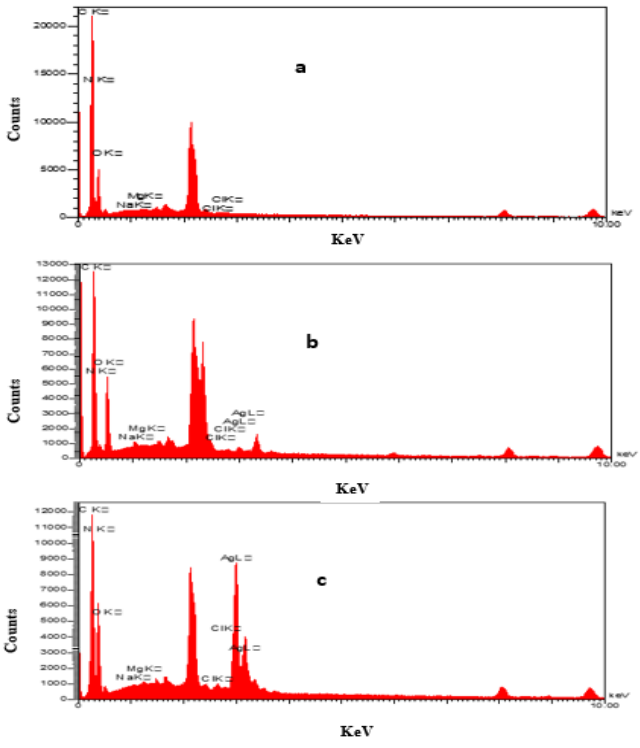

Figure 4. Elemental analysis of synthetic graphitic carbon nitride nanoparticles (a), graphene oxide nanoparticles (b), AC/CN/GO ternary composite using EDX spectroscopy (c)

The effect of different factors on the reaction of synthesized nanocomposites
Solutions with different pHs of 1.5, 1.5, 2.5, 2.3, 3.5 were prepared with a concentration of 15 ppm and then the absorbance was recorded in the UV device before adding the adsorbent and the absorption percentage was obtained using the absorption percentage relationship [Fig. 5].

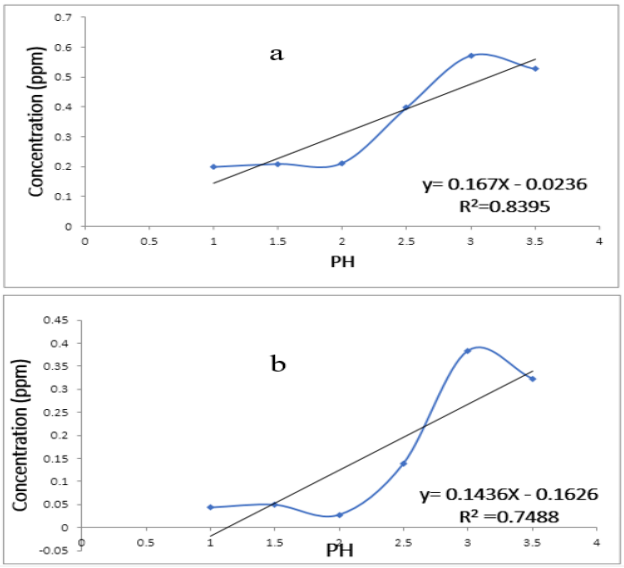

Figure 5. Regression diagram before adsorption during maximum (a), Regression diagram after absorption along the maximum (b)

Investigate the different effect of ternary nanocomposite Ag_2CO_3 / GO / g-C_3N_4 on the removal of methyl orange
The UV device recorded absorptions in six flasks each containing 30 ml of methyl orange solution with a concentration of 15 ppm at 3 pHs with different amounts of adsorbent in a shaker for 30 minutes and then, in the centrifuge with 4000 revolutions and a time of 4 minutes to investigate the effect of different amounts of adsorbent (triple nanocomposite) in removing methyl orange from the aqueous medium, and the corresponding graph was drawn in Excel. According to the figure 6, the maximum absorption is in the amount of 0.02 grams, i.e. 20 mg of the adsorbent.

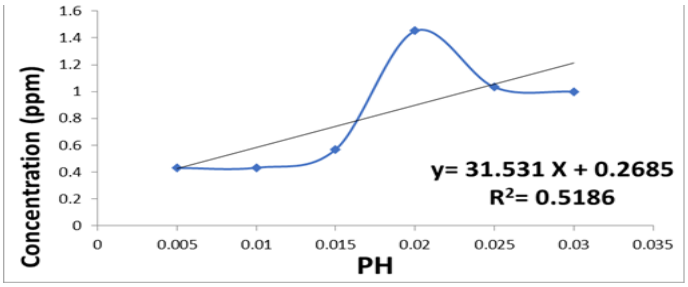

Figure 6. Absorbent optimal regression diagram along the maximum

The effect of time investigation on the removal of methyl orange
The number of 6 flasks containing the equal amounts of 30 ml of methyl orange solution with a concentration of 15 ppm and adsorbent with an amount of 0.02 grams per time was placed in a shaker for 30 to investigate the effect of different times in the removal of methyl orange using ternary nanocomposite AC/GO/CN adsorbent, and every 5 minutes, the contents of one of the flasks were filtered in a centrifuge tube for 4 minutes at 4000 rpm, and the corresponding absorption was measured in the UV-VIS device. The maximum absorption took place in 25 minutes [Fig. 7].

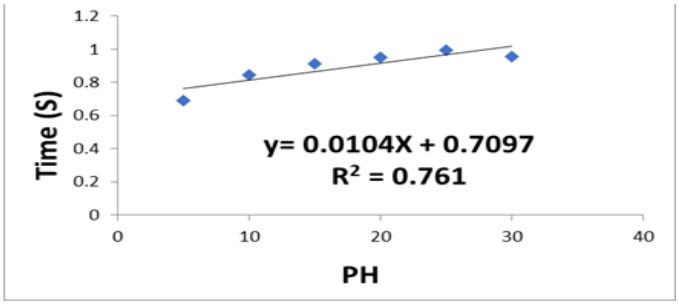

Figure 7. Optimal time regression diagram during max
The effect of methyl orange removal in different concentrations

Ternary nanocomposite AC/GO/CN was investigated in the removal of different concentrations of methyl orange at pH = 3 and in a contact time of 25 minutes [Fig. 8]. For this purpose, 0.02 grams of ternary nanocomposite was added to each of the 30 ml of 2, 5, 8, 13, 15, 20 ppm methyl orange solution in 6 jars with different concentrations. Then it was stirred for 25 minutes in a shaker at 250 rpm, then it was smoothed in a centrifuge for 4 minutes at 4000 rpm, then the UV-VIS device values were recorded before and after absorption followed by plotted graphs.

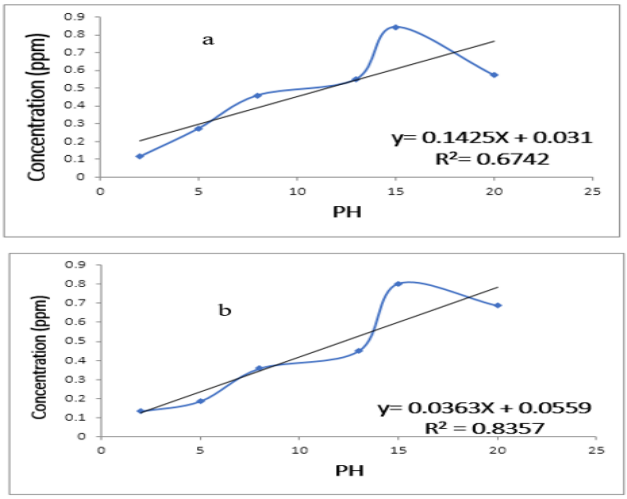

Figure 8. Optimal regression diagram before adsorption during maximum (a) Optimal concentration regression diagram after adsorption during maximum (b)

Adsorption isotherms are widely used to understand the type of adsorbent-adsorption interaction, especially for the removal of dye pollutants. The isothermal data can be fitted with different isothermal models so that to present a suitable model for investigating the process. The value of correlation coefficient R^2 obtained from Langmuir, Temkin and Freundlich absorption isotherms for methyl orange was investigated, with best R^2 line corresponding to Langmuir. Isotherms were drawn using the data and the results of the experiments on Langmuir, Freundlich, and other relevant diagrams for methyl orange [Fig. 9].

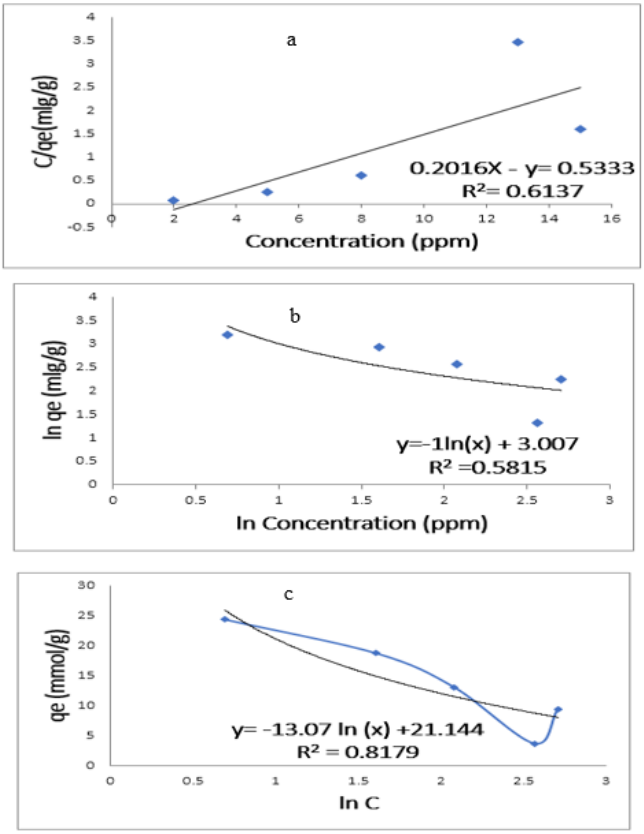

Figure 9 . Langmuir isotherm for adsorption of methyl orange by triple nanocomposite (ph = 3, adsorbent amount of 0.02 g in 25 minutes) (a), Freundlich isotherm for adsorption of methyl orange by triple nanocomposite (pH = 3, adsorbent amount of 0.02 g in 25 minutes) (b), Absorption isotherm of methyl orange adsorption by triple nanocomposite (ph = 3, adsorbent amount of 0.02 g in 25 minutes) (c)

The study of adsorption kinetics is important because it provides valuable information about the mechanism of adsorption reactions. The contact time of the adsorbent and methyl orange is one of the main parameters affecting the efficiency and speed of the degradation process. Methyl orange adsorption kinetic data were fitted to pseudo-first-order and pseudo-second-order kinetic models. Considering that the pseudo-second order kinetic model shows a good correlation between the speed constant and the q value [Fig. 10].

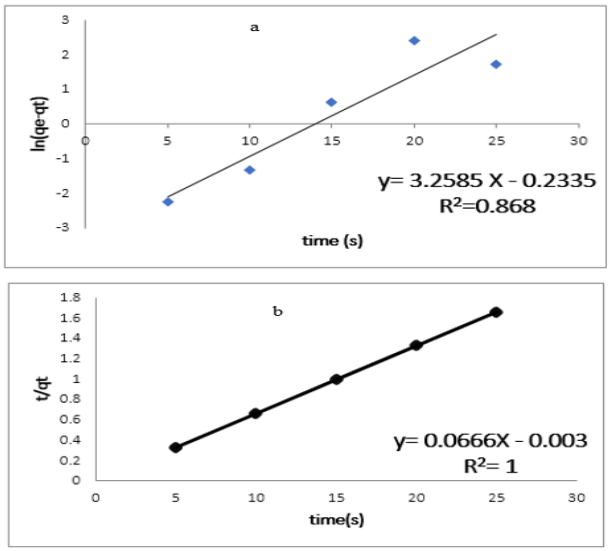

Figure 10. Quantitative first-order kinetics of methyl orange adsorption by AC / GO / CN triple nanocomposite (pH 5, adsorbent value 0.02 g, concentration 15ppm, time 25 minutes) (a), Quasi quadratic kinetics diagram of methyl orange adsorption by AC/GO/CN triple nanocomposite (pH 5, adsorbent value 0.02 g, concentration 15ppm, time 25 minutes) (b)

Equilibrium Adsorption Studies

Langmuir Adsorption Isotherm

The Langmuir model assumes monolayer adsorption on a homogeneous surface. The governing equation is given by: [٥٥]

$$q_e = \frac{q_{max} b C_e}{1 + bc_e}$$

$$\frac{C_e}{q_e} = \frac{1}{q_{max} b} + \frac{C_e}{q_{max}}$$

q_e: Amount of dye adsorbed at equilibrium

q_{max}: Maximum adsorption capacity

b: Langmuir constant (1/mmol)

By plotting q_e/C_e versus C_e, the slope yields q_{max}, and the intercept gives the Langmuir constant b.

Figure (11) shows the Langmuir isotherm for methyl orange adsorption onto the CN/GO/AC ternary nanocomposite under optimal conditions.

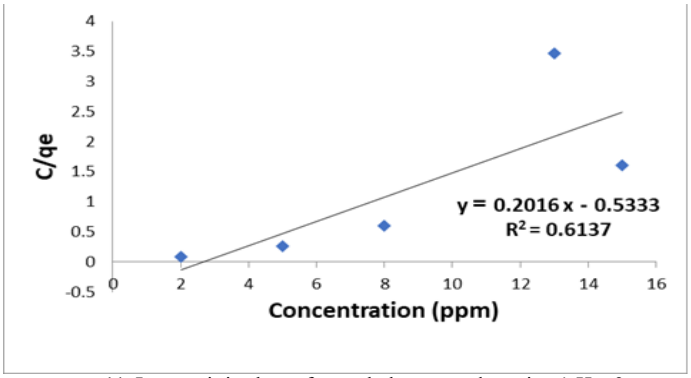

Figure 11. Langmuir isotherm for methyl orange adsorption (pH = 3, adsorbent dosage = 0.02 g, contact time = 25 min)

Freundlich Adsorption Isotherm

The Freundlich isotherm describes multilayer adsorption on heterogeneous surfaces[٥٦].

$$q_e = k_F . Ce^{1/n}$$

Its logarithmic form is:

$$Log q_e = Log k_f + \frac{1}{n} Log C_e$$

K_f and n: Freundlich constants, indicating adsorption capacity and intensity, respectively.

Given that the coefficient of determination (R^2) for the Langmuir model was higher than that of the Freundlich model, the experimental data better fit the Langmuir isotherm. Figure 14 illustrates the Freundlich isotherm for methyl orange adsorption onto the CN/GO/AC nanocomposite under optimal conditions [Fig. 12].

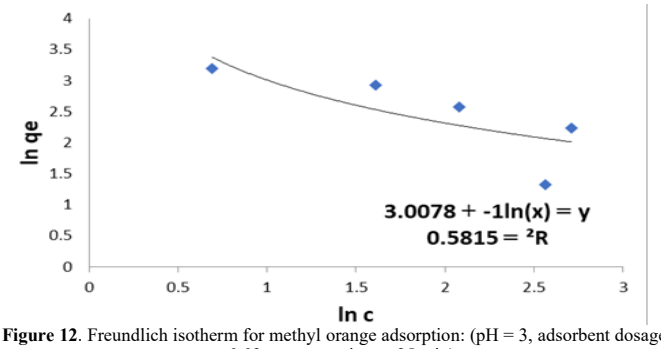

Figure 12. Freundlich isotherm for methyl orange adsorption: (pH = 3, adsorbent dosage = 0.02 g, contact time = 25 min)

The Temkin isotherm incorporates a factor that reflects the interaction between the adsorbent and the adsorbate. The model is defined as follows: [٥٧]

$$q_e = \frac{RT}{b} ln(AC)$$

$$\frac{RT}{b} = B$$

The linear form of the Temkin isotherm is expressed as follows:

$$q_e = BlnA + BlnC_e$$

In this equation:

A (g/L) is the equilibrium binding constant related to the maximum adsorption energy.

B (dimensionless) is proportional to the heat of adsorption.

b (J/mol) is the Temkin constant.

Figure (13) illustrates the Temkin isotherm for methyl orange adsorption onto the CN/GO/AC ternary nanocomposite under optimal conditions.

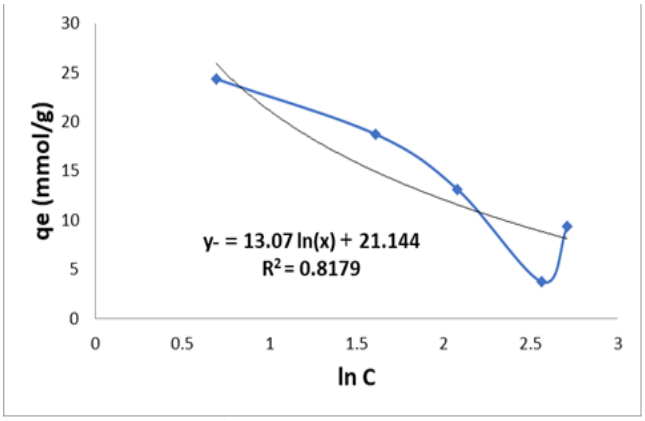

Figure 13. :(pH = 3, adsorbent dose = 0.02 g, contact time = 25 minutes)

Adsorption Kinetics Analysis

3. 9. 1. Pseudo-First-Order Kinetics

The Lagergren equation for pseudo-first-order kinetics is given by: [٥٨]

$$\frac{dq_1}{dt} = k_1(q_e - q_t)$$

Upon integration under the initial condition ($q_t = 0$ at $t = 0$ and $q_t = q_t$ at $t = t$),

$$log\left[\frac{q_e}{q_e - q_t}\right] = \frac{k_1}{2.303} t$$

the equation can be rearranged into its linear form:

$$\log(q_e - q_t) = log\ q_e - \frac{k_1}{2.303} t$$

$q_t - q_e$: amount of dye adsorbed at time t relative to the equilibrium amount

K_1: pseudo-first-order rate constant (1/min)

By plotting log ($q_t - q_e$) versus time (t), K_1 is obtained from the slope and q_e (predicted by the model) from the y-intercept.

Figure 14 presents the pseudo-first-order kinetic curve for methyl orange adsorption by the CN/GO/AC nanocomposite.

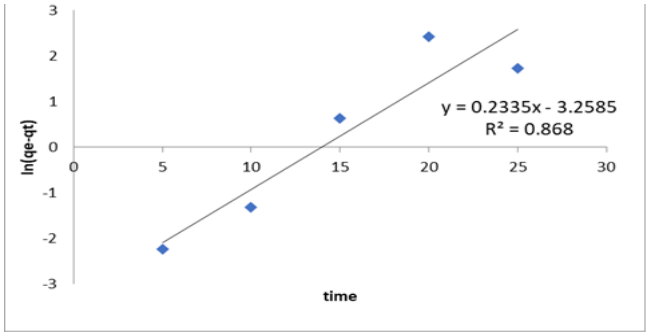

Figure 14. pseudo-first-order kinetic curve for methyl orange adsorption (pH = 0.5, adsorbent dose = 0.02 g, initial concentration = 15 ppm, contact time = 25 minutes)

Pseudo-Second-Order Kinetics

The Ho–McKay model for pseudo-second-order kinetics is described by: [۵۹]

$$\frac{dq_t}{dt} = k_2(q_e - q_t)$$

After integration and rearrangement, the linear form is:

$$\frac{1}{q_e - q_t} = \frac{1}{q_e} + k_2 t$$

$$\frac{1}{q_t} = \frac{1}{k_2 {q_e}^2} + \frac{1}{q_e} t$$

K_2: pseudo-second-order rate constant (g/mg·min)

q_e and q_t: amounts of adsorbate at equilibrium and at time t, respectively

From the linear plot of t/q_t versus t, K_2 and q_e can be calculated from the slope and intercept, respectively.

$$h = k{q_e}^2$$

h: the initial adsorption rate (mg/g.min), determined when $q_t/t \to 0$

Figure 15 displays the pseudo-second-order kinetic curve for methyl orange adsorption by the CN/GO/AC ternary nanocomposite.

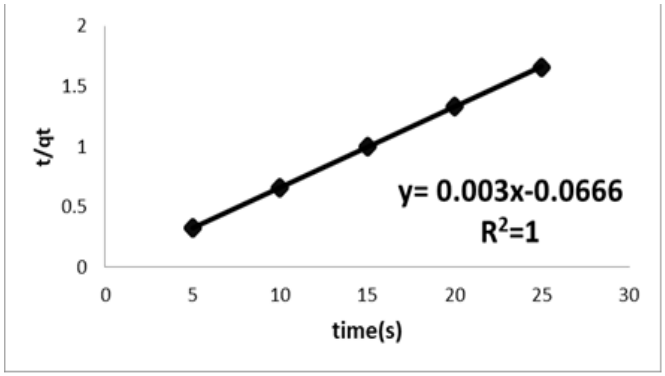

Figure 15. (pH = 0.5, adsorbent dose = 0.02 g, initial concentration = 15 ppm, contact time = 25 minutes)

4.Conclusions

This paper synthesized, ternary nanocomposite $Ag_2CO_3/GO/C_3N_4$. The structure of nanoparticles was confirmed by XTD pattern and the size of nanoparticles was determined by SEM images. Also, an important pollutant in the textile industry, namely methyl orange, was removed using ternary nanocomposite AC/GO/CN adsorbent in aqueous environment. Moreover, the optimal conditions were determined by examining the efficiency of nanocomposite in removing methyl orange from aqueous solutions. Also, various parameters such as pH, contact time of adsorbent and pollutant, initial concentration of pollutant and amount of adsorbent were investigated to achieve the best conditions for the removal of this dye. Graphene oxide as a metal- free material has attracted the attention of public attention due to its thin layer structure, high stability and high mobility. In addition, the metal nanoparticles supported by go have advanced catalytic performances because metal nanoparticles have good dispersion of edges and go surfaces. Compared to graphene, the surface of Go nanoparticles has more active groups, such as hydroxyl groups and carboxyl groups. Hence, many of the three with go were used as catalyst in the area. In this study, three GO / AC / CN composites were prepared via simple chemical precipitation method at ambient temperature. a set of techniques were used to study the characteristics of the CN / AC / GO, such as XRD, TEM, FTIR. For this reason, MO was selected as the target contaminant for the AC / CN / GO. According to the obtained results, the prepared nanocomposite has a favorable efficiency for the removal of methyl orange dye. The highest removal percentage for this pollutant is 92.5%. Also, the results of absorption isotherms showed that the absorption of this dye follows the Langmuir isotherm model. The reason for the increase in the efficiency of methyl orange removal with increasing the amount of adsorption can be attributed to the increase in the number of methyl orange adsorption sites on the surface of the adsorbent with increasing the amount of adsorbent, which itself increases the surface area. However, the surface of the adsorbent is saturated with methyl orange in the presence of small amounts of adsorbent. This saturation of the surface with methyl orange reduces the removal of dye, and thus methyl orange remains in solution in large amounts.Therefore, increasing the amount of adsorption creates more active sites for methyl orange binding and the efficiency also increases. On the other hand, after a certain amount of adsorbent, the adsorption capacity remains almost constant, which is due to the presence of hydrostatic interactions between the adsorbent sites, which are created as a result of increasing the amount of adsorbent and cause the active sites on their surface to be affected.

In this case, the maximum adsorption capacities under optimal conditions of the experimental data were better described by pseudo-second-order tick-tick equations, which were used to investigate the Langmuir and Freundlich isotherm studies, which also showed that the adsorption isotherm results deviate from the Langmuir isotherm model.

References

[1] U. Pagga and K. Taeger, *Water Research*, 1994, **28**, 1051–1057.
[2] U. Pagga and K. Taeger, *Water Research*, 1995, **29,** 1125–1130.
[3] C. A. Gouvêa, F. Wypych, S. G. Moraes, N. Durán, and P. Peralta-Zamora, *Chemosphere*, 2000, **40**, 427–432.
[4] C. C. Chen, W. H. Ma, and J. C. Zhao, *Chemical Society Reviews*, 2010, **39**, 4206–4219.
[5] C. S. Pan, J. Xu, Y. Chen, and Y. F. Zhu, Applied Catalysis B: *Environmental*, 2012, **115**–116, 314–322.
[6] A. Faisal, M. Y. Hafiz, Y. Umer, S. Aimon, H. Ejaz, A. M. Osama, I. Munawar, I. Faiza, A. A. R. Mustafa, and P. Muhammad, *Materials Chemistry and Physics*, 2025, **332**, 115789.160-178.
[7] S. Dawood, T. K. Sen, and C. Phan, *Water, Air, & Soil Pollution*, 2014, **225**, 1818.
[8] M. T. Yagub, T. K. Sen, S. Afroze, and H. M. Ang, *Advances in Colloid and Interface Science,* 2014, **209**, 172–184.
[9] A. Ghaly, R. Ananthashankar, M. Alhattab, and V. Ramakrishnan, *Journal of Chemical Engineering & Process Technology*, 2014, **5**, 182.
[10] A. M. Azeem, W. Jakub, N. M. Salman, and N. M. Tayyab, *Proceedings of Nanocon* 2016, 231–236.
[11] R. Sandoval, A. M. Cooper, K. Aymar, A. Jain, and K. Hristovski, *Journal of Hazardous Materials*, 2011, **193**, 296–303.
[12] I. Shafiq, M. Hussain, N. Shehzad, I. M. Maafa, P. Akhter, S. Shafique, A. Razzaq, W. Yang, M. Tahir, and N. Russo, *Journal of Environmental Chemical Engineering*, 2019, **7**,103265. 1–10.
[13] P. Wang and I. M. Lo, **Water Research**, 2009, **43**, 3727–3734.
[14] V. K. Singh and P. N. Tiwari, *Journal of Chemical Technology & Biotechnology*, 1997, **69**, 376–382.
[15] J. Fu, Z. Chen, M. Wang, S. Liu, J. Zhang, R. Han, and Q. Xu, *Chemical Engineering Journal*, 2015, **259**, 53–61.
[16] M. E. Olya and A. Pirkarami, *Separation and Purification Technology*, 2013, **118**, 557–565.
[17] M. E. Olya, M. Vafaee, and M. Jahangiri, *Journal of Saudi Chemical Society*, 2017, **21**, 33–41.
[18] M. E. Olya, A. Pirkarami, M. Soleimani, and M. Bahmaei, *Journal of Environmental Management*, 2013, **121**, 210–219.
[19] S. Karimi, M. Tavakkoli, R. R. Yaraki, and A. Karri, *Renewable and Sustainable Energy Reviews*, **2019**, **107**, 535–547.
[20] P. Sirajudheen et al., International *Journal of Biological Macromolecules,* 2020, **161**, 1117–1129.
[21] M. N. Ahmed and R. N. Ram, *Environmental Pollution*, 1997, 77, 79–86.
[22] S. Banerjee et al., Arabian *Journal of Chemistry*, 2019, **12**, 4051–4061.
[23] C. Wang et al., Chinese *Journal of Chemical Engineering*, 2009, **17**, 513–520.
[24] S. S. Tahir and N. Rauf, *Journal of Environmental Sciences*, 2006, **18**, 199–204.
[25] M. M. Hasan *et al*., *Journal of Molecular Liquids*, 2021, **323**, 1–12.
[26] Md. M. Hossain *et al*., *Journal of Molecular Liquids*, 2020, **319**, 1–11.
[27] V. Gómez and M. S. Larrechi, *Talanta*, 2007, **69**, 694–701.
[28] A. M. Herrera-González, M. Caldera-Villalobos, and A.-A. Peláez, *Journal of Environmental Management*, 2019, **234**, 480–488.
[29] M. Naushad *et al*., *Journal of Molecular Liquids*, 2019, **296**, 12–22.
[30] A. Chakraborty et al., *Journal of Colloid and Interface Science*, 2011, **359**, 228–239.
[31] P. Nautiyal and K. A. Subramanian, *Journal of Environmental Management*, 2016, **182**, 297–305.
[32] Y. Qiu., *Bioresource Technology*, 2009, **100**, 5342–5348.
[33] E. A. Sackey et al., *Environmental Technology*, 2021, 16, 102–110.
[34] D. A. G. Sumalinog, S. C. Capareda, and M. D. G. de Luna, *Journal of Environmental Managemen*t, 2018, **210**, 255–263.
[35] M. S. Islam, H. Roy, T. Ahmed, S. H. Firoz, and S. X. Chang, *Chemosphere*, 2023, **340**, 139827.100-112.

[36] M. A. Ahmed, E. E. El-Katori, and Z. H. Gharni, Journal of Hazardous Materials, 2013, 553, 19–28.
[37] S. Saha and J. M. A. Wang, *Separation and Purification Technology*, 2012, 89, 147–155.
[38] M. A. Behnajady and N. Modirshahla, Photochemical & Photobiological Sciences, 2006, 5, 1078–1081.
[39] M. Saquib and M. Muneer, *Dyes and Pigments*, 2003, **56**, 37–49.
[40] H. Y. Liu et al., *Photocatalysis Today*, 2019, **12**, 85–94.
[41] J. Z. Chen, *Advanced Oxidation Technologies*, 2017, **20**, 170–178.
[42] M. D. R. Al-Mamun et al., *Environmental Nanotechnology, Monitoring & Management*, 2021, **16**, 100519.45-55.
[43]. M.D. Rashid Al-Mamun, M.D. Shofikul Islam, M.R. Hossain, S. Kader, *M.D.S.* Islam, Z.H. Khan, *Environmental Nanotechnology, Monitoring & Management*, 2021.
[44] G. Crini, *Bioresource Technology*, 2006, **97**, 1061-1085.
[45]O. E. A. Salam, N. A. Reiad, and M. M. ElShafei, *Journal of Advanced Research*, 2011, **2**, 297–304.
[46] M. F. Hassan, M. A. Sabri, H. Fazal, A. Hafeez, N. Shezad, and M. Hussain, *Journal of Analytical and Applied Pyrolysis*, 2020, **145**, 104715.
[47] C. Liang, C. G. Niu, H. Guo, D. W. Huang, X. J. Wen, S. F. Yang, and G. M. Zeng, *Catalysis Science & Technology*, 2018, **8**, 1161–1169.
[48] Y. Zhu, S. Murali, W. Cai, X. Li, J. W. Suk, J. R. Potts, and R. S. Ruoff, *Advanced Materials*, 2010, **22**, 3906–3924.
[49] M. Handayani, Y. Mulyaningsih, A. Anggoro, M. Abbas, A. Setiawan, and I. Triawan, *Materials Letters*, 2022, 314, 11–22.
[50] N. Sykam, V. Madhavi, and G. M. Rao, Journal of Environmental Chemical Engineering, 2018, **6**, 3223–3231.
[51] M. A. Karimi, H. Aghaei, and V. Nezhadali, *Materials Electronics*, 2019, **30**, 6300–6308.
[52] N. Jahan, H. Roy *et al*., *Case Studies in Chemical and Environmental Engineering*, 2022, 6, 15–32.
[53] H. Y. Liu, C. Liang, C. G. Niu, D. W. Huang, Y. B. Du, H. Guo, L. Zhang, Y. Y. Yang, and G. M. Zeng, *Applied Surface Science*, 2019, **475**, 421–430.
[54] S. Nasiri, M. Rabiei, A. Palevicius, G. Janusas, A. Vilkauskas, V. *Nutalapati, and A. Monshi, Nano Trends*, 2023, **3**, 1–9.
[55] N. S. A. Mubarak,. Y. Liu, C. Liang, C. G. Niu, D. W. Huang, Y. B. Du, H. Guo, L. Zhang, Y. Y. Yang, and G. M. Zeng, *Applied Surface Science*, 2019, **475**, 421–430.
[56] A. Mittal, A. Malviya, D. Kaur, J. Mittal, and L. Kurup, *Journal of Hazardous Materials*, 2007, **148**, 229–240.
[57] S. A. Akolo and A. S. Kovo, *Journal of Encapsulation and Adsorption Sciences*, 2015, **5**, 21–29.
[58] E. Z. Villafranco, D. Icela, B. Quintal, S. Gomez-Salazar, M. Barceló-Quintal, E. Hugo, S. Correa, and J. M. Soriano-Rodríguez, *Journal of Environmental Protection*, 2014, **5**, 608–617.
[59] F. S. Atsar, D. Kukwa, R. A. Wuana, and B. Arwenyo, *American Journal of Analytical Chemistry*, 2021, **12**, 145–154.